J. Fluid Mech. (2007), *vol.* 588, *pp.* 29–41.
doi:10.1017/S0022112007007069 Printed in the United Kingdom

Gravity-driven reacting flows in a confined porous aquifer

JAMES VERDON AND ANDREW W. WOODS

BPI, Madingley Rise, Madingley Road, University of Cambridge, Cambridge CB3 0EZ, UK

(Received 29 September 2006 and in revised form 13 March 2007)

We develop a model for the dynamics of a reactive gravity-driven flow in a porous layer of finite depth, accounting for the change in permeability and density across the dissolution front. We identify that the two controlling parameters are the mobility ratio across the reaction front and the ratio of the buoyancy-driven flow to the fluid injection rate. We present some numerical solutions for the evolution of a two-dimensional dissolution front, and develop an approximate analytic solution for the limit of large injection rate compared to the buoyancy-driven flow. The model predictions are compared with some new analogue laboratory experiments in which fresh water displaces a saturated aqueous solution initially confined within a two-dimensional reactive permeable matrix composed of salt powder and glass ballotini. We also present self-similar solutions for an axisymmetric gravity-driven reactive current moving through a porous layer of finite depth. The solutions illustrate how the reaction front becomes progressively wider as the ratio of the buoyancy-driven flow to the injection rate increases, and also as the mobility contrast across the front increases.

1. Introduction

Many natural and industrial processes involve the flow of reactive fluids through permeable rock (Phillips 1991; Liu *et al.* 1997). The dynamics and instabilities of such reaction fronts in pressure-driven flow have been studied in detail, especially owing to their interest in the dissolution of mineral precipitate near oil wells (Ortoleva *et al.* 1987; Liu *et al.* 1997; Chen *et al.* 1997). Often the reaction fronts can become unstable leading to the formation of a highly fingered interface, and ultimately the formation of dissolution channels or wormholes (Daccord, Lenormand & Lietarel 1993*a*, *b*; Golfier *et al.* 2002; Fredd & Fogler 1999). However, in many natural situations, buoyancy contrasts may play a key role in the dynamics as fluid spreads through confined permeable strata (Barenblatt 1996; Nigam & Woods 2006). If an advancing gravity-driven flow reacts with the rock, leading to partial dissolution, then there will be an increase in permeability behind the reaction front, which in turn can have a dynamic feedback on the flow. Examples of such flow may arise if fresh water is injected into a saline aquifer for storage (Bear 1972; Mitchell & Woods 2006), or if cold surface water is injected into a geothermal reservoir to mine additional heat (Woods 1999; Menand, Raw & Woods 2002; Jupp & Woods 2003, 2004). In both cases, the injected water may be unsaturated in minerals present in the rock. Recently, interest has also focused on the injection of CO_2 into saline aquifers as part of the process of CO_2 sequestration (Lagneau, Pipart & Catalette 2005; Nordbotten & Celia 2006). At the high pressures of deep saline aquifers, CO_2 is in supercritical form, and as it migrates through an aquifer, displacing water, it will mix with residual water in

the pore spaces. This juxtaposition of CO_2 and H_2O may generate fluids which are highly reactive with carbonate minerals if the pH of the reactive fluid remains low. In this case, the associated dissolution reactions may increase the permeability by factors of 10–100 (Grigg, McPherson & Svec 2003). Note however, that in non-carbonate rocks, reaction rates may be much slower, and the kinetics of dissolution may become the rate-limiting control on any fluid–rock reactions (e.g. Lagneau *et al.* 2005).

The purpose of this work is to explore the feedback of such reactions on the gravity-driven flow of a liquid through a confined permeable rock. We focus on the idealized situation in which an unsaturated aqueous solution is injected into a confined horizontal aquifer. We assume the aquifer is initially filled with saturated aqueous solution, and we consider the case in which a small fraction of the solid porous matrix, for example the intergrain cement, is soluble in the fluid (Phillips 1991). We develop a simple analogue laboratory model of this situation using aqueous solutions moving through a porous medium composed of glass ballotini and a small mass of salt powder. As the unsaturated fluid moves through the pore spaces, a dissolution front develops across which that fraction of the matrix which is soluble dissolves into the fluid (Phillips 1991; Jupp & Woods 2003). If the time for reaction is fast compared to the time for the fluid to move through the pores, as is the case with some highly reactive carbonate minerals (Golfier *et al.* 2002) and also in our experiments, then the front will be localized (Phillips 1991), and we consider this limit herein. For simplicity, as in our experiments, we also assume that the reacted fluid ahead of the front is of comparable density with the original fluid in the porous matrix, and of greater density than the unreacted injected liquid advancing towards the reaction front.

Earlier studies have examined the motion of gravity-driven reaction fronts in unconfined permeable layers (Raw & Woods 2003). Here we show that when the layer has a finite depth, the motion of the original fluid is key because as the reaction front develops it intersects both the upper and lower boundary of the permeable layer, thereby displacing the original fluid. We first present an analysis of a two-dimensional flow, corresponding to injection of fluid from a horizontal well into a confined permeable layer (figure 1*a*). The model equations are analogous to the classical model for fluid–fluid displacement in a porous layer (cf. Bear 1972), although it has a different interpretation in the present context of a gravity-driven reaction front. We compare the model predictions to the results of our new analogue laboratory experiments. We then extend the analysis to consider the flow spreading from a vertical injection well, which can lead to an axisymmetric reaction front spreading around the well. In this latter situation, we develop some new similarity solutions for the shape of the reaction front, following the approach of Nordbotten & Celia (2006) and Mitchell & Woods (2006). We conclude with a short discussion of some of the implications of our results.

2. Model of the flow in a reactive confined aquifer

The motion of a gravity-driven reaction front can be modelled using Darcy's law for flow in a porous medium, combined with a relation for conservation of salt across the reaction front (Phillips 1991). The schematic in figure 1(*a*) illustrates the morphology of the current, and the variables used in our model. As the current spreads out under the upper surface of the aquifer, $y = H$, we assume that the vertical velocity is small compared to the horizontal velocity and so the vertical pressure gradient is close to hydrostatic (Barenblatt 1996)

$$P(x, y, t) = p(x, t) - \rho g y \quad \text{for} \quad 0 < y < h \tag{1a}$$

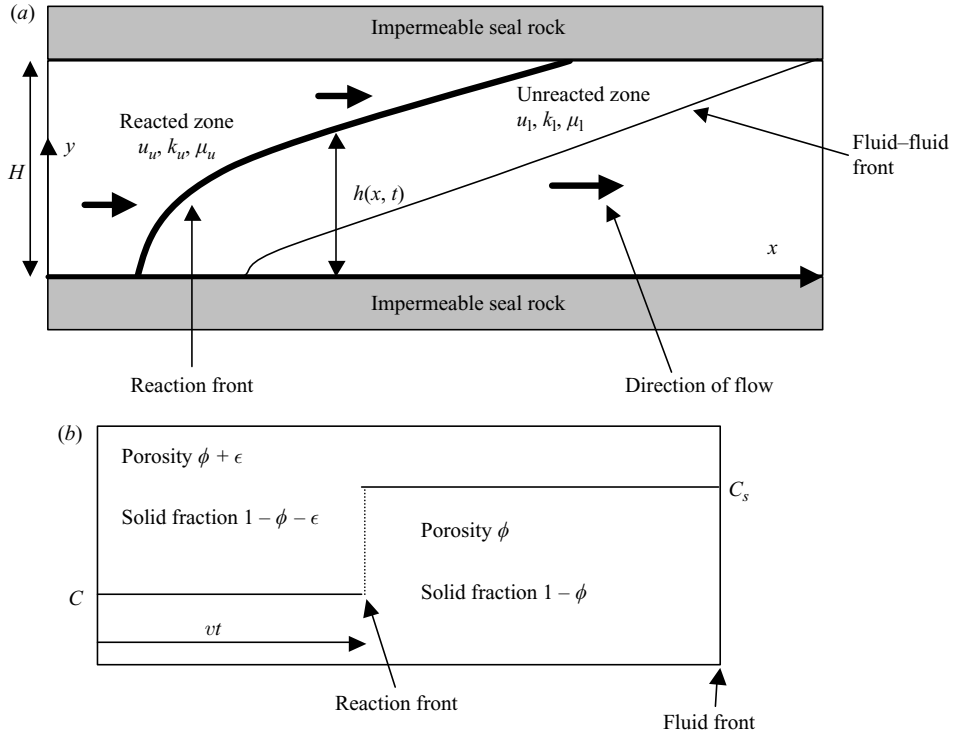

FIGURE 1. (*a*) Schematic of the two-dimensional flow geometry, illustrating the reaction front and the fluid–fluid front. (*b*) Cartoon to illustrate the conservation of salt across the reaction front.

and

$$P(x, y, t) = p(x, t) - \rho g y + \Delta\rho g(y - h) \quad \text{for} \quad h < y < H. \tag{1b}$$

Here $p(x, t)$ is the pressure on the lower boundary of the aquifer, h is the height of the reaction front above the lower boundary of the aquifer, and $\Delta\rho$ is the density contrast between the saturated fluid ahead of the front and the unsaturated fluid behind the front. Combining this pressure distribution with Darcy's Law for the flow leads to expressions for the Darcy velocity in the zone of unreacted fluid behind the reaction front,

$$u_u = -\frac{k_u}{\mu_u}\left[\frac{\partial p}{\partial x} - \Delta\rho g \frac{\partial h}{\partial x}\right] \quad \text{for} \quad H > y > h, \tag{2a}$$

and the zone of reacted or salt saturated fluid ahead of the reaction front

$$u_l = -\frac{k_l}{\mu_l}\frac{\partial p}{\partial x} \quad \text{for} \quad h > y > 0. \tag{2b}$$

Here u denotes Darcy velocity, H is the thickness of the aquifer, μ is the fluid viscosity, ϕ the porosity and k the permeability. Subscripts u and l denote the upper, unreacted zone of fluid ($y > h$) behind the reaction front and the lower, reacted zone of saturated fluid ($y < h$) ahead of the reaction front.

We now combine these relations with an expression for the conservation of salt (or other soluble mineral) across the reaction front to establish a relation between the speed of the reaction front and the fluid (figure 1*b*). First, we assume there is a volume

of salt $\epsilon \ll 1$, per unit volume of the rock, which is soluble in the liquid, so that prior to the reaction, the solid volume fraction is $1-\phi$ and after reaction, the solid volume fraction is $1-\phi-\epsilon$. We denote the salt density as S, and assume the salt dissolved in the aqueous solution has a mass per unit volume C in the unsaturated (upper layer) and C_s in the saturated (lower layer) fluid. The speed of the reaction front, v, may then be found by analysis of the conservation of salt in the injected fluid. Essentially at time t, a mass $M_i = uCt$ of salt has been injected from the source, while the mass of salt in solution in the injected fluid is $M_s = (\phi+\epsilon)vCt + (u-(\phi+\epsilon)v)tC_s$. The difference between these quantities, $M_s - M_i = (u-(\phi+\epsilon)v)(C_s - C)t$ represents the mass of salt that has been dissolved from the solid matrix. By equating this with a direct expression for the mass of salt dissolved from the rock, ϵvSt, we deduce that

$$v = \frac{u(C_s - C)}{(\epsilon S + (\phi+\epsilon)(C_s - C))} = \lambda u. \tag{3}$$

It is also relevant to note that, in this model, the fluid injected into the rock extends a distance $(u-\epsilon v)t/\phi$ from the source, and the original fluid lies ahead of this point. In the present application, we are concerned with the case in which $\epsilon \ll 1$ so that there is little change in the porosity associated with the dissolution. However, the permeability may change more significantly if the salt which dissolves originally fills part of the throats between the pores.

To calculate the shape of the current, we now adopt the extended Boussinesq approximation, in which we neglect changes in density of the liquid except in the buoyancy forces and we neglect changes in the porosity across the reaction front, except its impact on the permeability (cf. Phillips 1991). Then, for a long and thin gravity-driven flow, the depth of the reacted zone above the reaction front, $H-h$, increases if the volume flux of unsaturated fluid decreases with distance from the source, according to the relation

$$\frac{\partial(H-h)}{\partial t} = -\lambda \frac{\partial}{\partial x}[(H-h)u_u]. \tag{4}$$

In the case of continuous steady injection, the total flow rate per unit width of the aquifer or experimental cell is given by

$$Q = (H-h)u_u + hu_l \tag{5}$$

and is constant. For constant flow, the above relations may be combined to form one governing equation for the dimensionless thickness of the reacted rock

$$\mathscr{H} = 1 - h/H \tag{6}$$

as a function of dimensionless position $\zeta = x/H$ and dimensionless time $\tau = tQ\lambda\beta/H^2$ (cf. Bear 1972):

$$\frac{\partial \mathscr{H}}{\partial \tau} + \frac{\partial}{\partial \zeta}\left[\frac{\mathscr{H}}{1+(\beta-1)\mathscr{H}}\right] = B\frac{\partial}{\partial \zeta}\left[\frac{\mathscr{H}(1-\mathscr{H})}{1+(\beta-1)\mathscr{H}}\frac{\partial \mathscr{H}}{\partial \zeta}\right] \tag{7}$$

where the dimensionless parameter B denotes the ratio of the gravity-driven flow and a uniform flow associated with the injection at rate Q per unit length,

$$B = \Delta\rho g H k_l/\mu_l Q, \tag{8}$$

and β is the dimensionless change in mobility across the reaction front,

$$\beta = \mu_l k_u / k_l \mu_u. \tag{9}$$

Typically $\beta > 1$ in a dissolution reaction. In an industrial context, injection rates may typically lie in the range $0.01-0.1\mathrm{m}^3\,\mathrm{s}^{-1}$ in a horizontal well of lateral extent 1000 m. For rocks of permeability 10^{-12}–$10^{-14}\,\mathrm{m}^2$ and thickness $H \sim 100\,\mathrm{m}$, with $\Delta\rho = 0.1-0.01\rho$ and $\mu_l \sim 0.001\,\mathrm{Pa\,s}$ then B has values in the range 10^{-6}–1.0, suggesting that the effects of gravity are small but non-negligible, especially in the deeper or more permeable layers.

In the limit $B \to 0$, equation (7) has an analytical solution for the depth of the reacted zone of rock given by $\mathscr{H}(\zeta, \tau)$,

$$\mathscr{H} = \frac{1}{\beta - 1}\left[\left(\frac{\tau - \tau_o}{\zeta - \zeta_o}\right)^{1/2} - 1\right] \quad \text{for} \quad \frac{\tau - \tau_o}{\beta^2} < \zeta - \zeta_o < \tau - \tau_o \tag{10}$$

while $\mathscr{H} = 1$ for $\zeta - \zeta_o < (\tau - \tau_o)/\beta^2$ and $\mathscr{H} = 0$ for $\zeta - \zeta_o > \tau - \tau_o$. In (10), $\mathscr{H}$ represents the depth of the reacted zone at a distance $\zeta = \zeta_o + (\tau - \tau_o)/(1 + (\beta - 1)\mathscr{H})^2$ downstream at time τ, given that the depth was $\mathscr{H}$ at the position ζ_o at time τ_o.

Note that equation (7) is analogous to the equation governing the average concentration of the fluid mixture when one fluid displaces a second miscible fluid of smaller mobility within a confined aquifer (e.g. Bear 1972; Yortsos & Salin 2006). In that different problem, the interface between the fluids becomes highly tortuous as fingers of the high-mobility fluid invade the low-mobility fluid. The fingered zone can be described in terms of the cross-aquifer-averaged concentration of the high-mobility fluid. The solution analogous to equation (10) then describes this mixed zone, in the limit of high Péclet number and hence negligible diffusivity. However, in contrast to the present gravity-controlled intrusion in which $\mathscr{H}$ describes the depth of the reacted zone at the top of the aquifer, with a miscible pressure-driven displacement, the fingers of the high-mobility fluid penetrate the low-mobility fluid on a range of length scales, across the whole interface. Comparison with experiments shows that in that context, the solution of the form of equation (10) overpredicts the rate of spreading of the mixed zone (Yortsos & Salin 2006). This is a result of the neglect of the cross-finger diffusion, which, in fact, acts to smear the interface between the two fluids, thereby changing the effective mobility of the fluid in the mixed zone.

However such a pressure-driven miscible displacement is somewhat different to the present problem in which (7) describes the advance of a reaction front as observed in our experiments (see the next section), and in which the change in mobility is associated with the change in the permeability of the matrix as well as any change in viscosity associated with the changing concentration of the fluid across the reaction front. The main point of contact of our problem with this earlier work is that in the limit of purely pressure-driven flow, corresponding to $B = 0$, the reaction front could in principle become unstable and highly tortuous (cf. Golfier *et al.* 2002). In that case, as the length scales of the fingers normal to the reaction front decrease, cross-front diffusion of solute could then smear the reaction front. However, in our experiments, we focus on the case with $B \sim O(1)$, in which there is a well-defined, gravity-controlled reaction front which becomes progressively thinner with distance from the source (figure 1*a*). In this case, cross-front diffusion is unlikely to be important except in very thin aquifers or once the flow has spread a very large distance, L, given by the scaling $L \sim H^2 u/D \sim 10^7\,\mathrm{m}$ where D is the solutal diffusivity, of order $10^{-9}\,\mathrm{m}^2\,\mathrm{s}^{-1}$, for a typical flow speed of order $u \sim 10^{-6}\,\mathrm{m\,s}^{-1}$.

Instead, in the present context, the solution given by equation (10) provides a reference as the theoretical limit in which there is no gravitational force and hence for which the leading edge of the reaction front spreads more slowly than with $B = O(1)$.

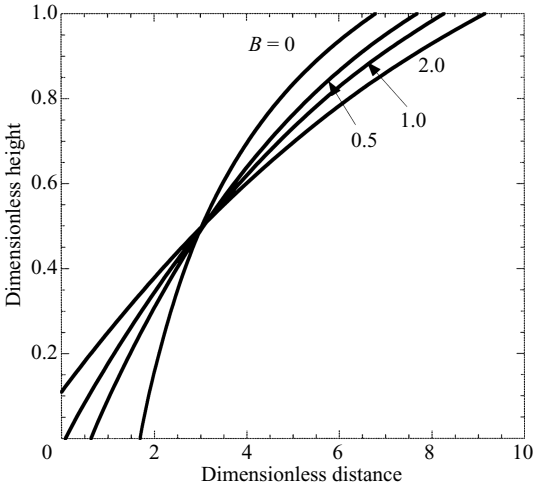

FIGURE 2. Illustration of the change in shape of the reaction front as a function of the parameter B, which measures the gravitational forces compared to the viscous resistance associated with the applied flow rate. The analytical solution ($B = 0$) is shown for comparison.

For example, in figure 2, we show numerical solutions of equation (7) for a range of values of B. These numerical solutions, calculated using a finite-difference formulation of equation (7) (Ames 1977), are shown at the same dimensionless time as for the analytical solution (10). For this comparison, we chose the initial reaction front to be close to vertical, $\mathscr{H}(\zeta_o, 0) = 1 - \zeta_o/\zeta_r$ for $0 < \zeta_o < \zeta_r$, with $\zeta_r = 0.1$. It is seen that (10) provides a good approximation for the numerical predictions of the position of the reaction front when $B \ll 1$. However, as B increases, the importance of gravitational spreading also increases, and the nose of the current propagates even further from the source.

The limiting solution given by equation (10) also identifies that at long times, as the influence of the initial conditions diminishes, the nose of the reaction front has position $\zeta \sim \tau$ which corresponds to the dimensional value $x \sim Q\lambda\beta/Ht$. This is a factor β larger than the theoretical distance a stable vertical reaction front would propagate. Noting the caveats about any cross-front diffusion (cf. Yortsos & Salin 2006), the solution illustrates the impact of the change in permeability and hence mobility, $\beta(> 1)$, across the reaction front on the lateral extent of the reaction zone.

3. Experimental model of a gravity-driven reaction front

To test the dissolution model, as distilled into the governing equation (7), we developed an analogue experimental system, in which we filled a small sealed Perspex cell with a mixture of glass ballotini, of diameter 100 micron, and salt powder. We used two cells, a short cell of dimensions 60 cm long $\times$ 10 cm high $\times$ 1 cm wide and a longer cell of dimensions 200 cm long $\times$ 10 cm high $\times$ 1 cm wide; the shorter cell was useful for initial visualization experiments, but the longer cell allowed us to compare the model with very long currents, up to 200 cm in lateral extent. In the experiments, we used very small mass fractions of salt in the range 0.05–0.1 of the total mass of matrix, so that the change in porosity associated with any dissolution is small. We used water as the working fluid so that the salt powder would dissolve, thereby increasing the porosity of the matrix by 2 %–5 %. This increase in porosity

is sufficient to produce a large change in the permeability of the matrix and hence the mobility of the fluid, but is sufficiently small that there is little compaction of the grains. Independent measurements of the mobility, before and after the reaction, were carried out in a calibration experiment. In the calibration experiment, the dry cell was filled with a mixture of glass ballotini and salt powder. The cell was then sealed and filled with saturated aqueous solution using the inflow/outflow vents at the two ends. In the first experiment, the cell was placed with the long axis vertical, and saturated aqueous solution was supplied to the top end of the cell from a source reservoir of known pressure. The fluid then migrated down through the cell and issued from the other end. The rate of outflow was measured to estimate the flow rate through the cell. In a second calibration experiment, the aqueous solution in the source reservoir was replaced with fresh water with the same source pressure. As the fresh water invaded the cell from above, a horizontal reaction front formed. The front remained stable owing to the relatively large change in density of the fluid across the front, and the front migrated slowly downwards through the reactive matrix. Once the reaction front had passed through the cell, the flow rate was again measured for a given pressure head driving the flow. Typical measurements of the two flow rates indicated a change in mobility across the horizontal reaction front by a factor $\beta \sim 1.9 \pm 0.2$. This value includes the effects of both a change in viscosity of the solution with salinity and also a change in permeability of the matrix as the salt is dissolved.

Prior to each reactive gravity current experiment, the cell was placed with the long axis horizontal and the intermediate axis vertical (figure 3*a*), filled with ballotini and salt powder, and then flooded with saturated saline solution. An inflow pipe connected to the upper part of one vertical endwall of the cell was then connected to a fresh water reservoir via a peristaltic pump. An outflow pipe at the other end of the cell allowed fluid to leave in response to the input from the pump. As water is pumped into the cell, the fresh water displaces the original saline water. Since it is buoyant, the fresh water tends to run through the upper part of the cell adjacent to the top boundary. The leading edge of the injected water is visualized by dying the injected water.

In the experiments, we observed that the fluid–fluid front is followed by a sharp reaction front, across which the salt powder originally in the cell dissolves into the fresh water. In the region behind the reaction front, there appears to be no salt in the matrix. Point measurements of the salinity of the fluid in the cell were taken by withdrawing small samples of the fluid through a series of small holes in the wall and into a syringe. These indicated a decrease in the salinity of the fluid, from saturated solution to pure water, as the reaction front passed by. Figure 3(*b*) shows a series of four photographs illustrating the time evolution of one typical experimental flow in the shorter experimental apparatus. The photographs were taken at times 208, 424, 670 and 850 s after the start of the experiment in which the flow rate was $0.26\,\mathrm{m^3\,s^{-1}}$. To help visualize the flow pattern, and the reaction front, the injected liquid is dyed and the colour of the dye is changed at various times. For the low flow rates used in the laboratory, the dissolution of salt appears to occur in a narrow zone around a well-defined reaction front. The reaction front is identified as a narrow interface region, $<$1–2 mm thick, across which there is a distinct change in light intensity, within the zone of injected liquid. This lies some distance behind the fluid–fluid front between the clear original interstitial fluid and the injected blue fluid.

The dye shows how the liquid migrates across the reaction front with time. The injected water is initially dyed blue, but this is changed to red at a later time in the experiment. Careful observation of the flow suggests that the most recently injected

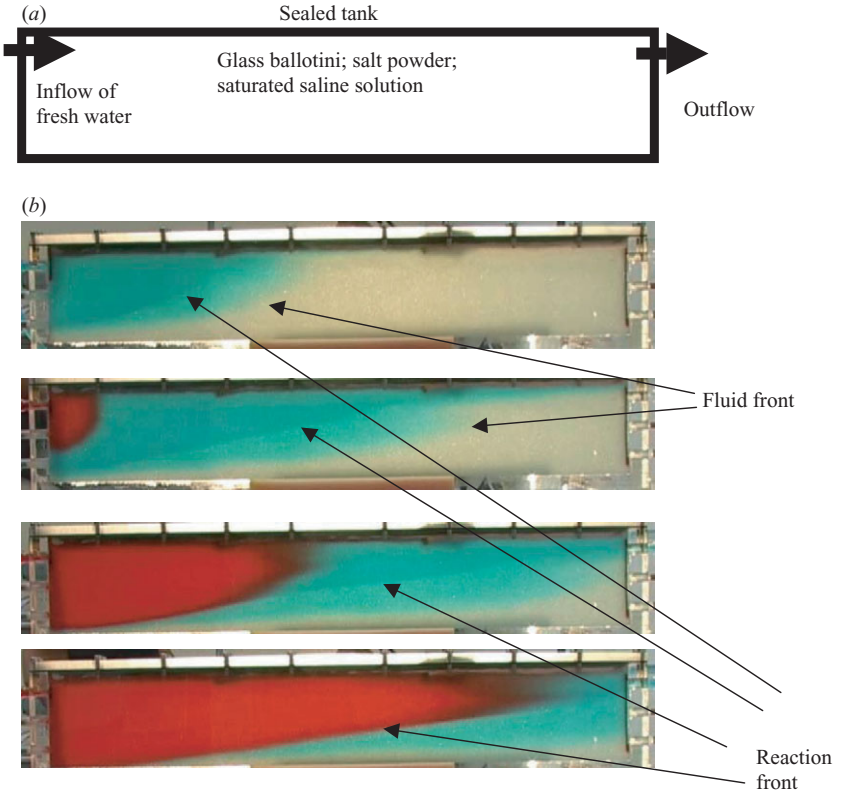

FIGURE 3. (*a*) Schematic of the experimental system. (*b*) Series of four photographs taken at times 208 s, 424 s, 670 s and 850 s, to illustrate the evolution of the reaction front and the motion of the fluid through the reacting porous cell. This experiment was conducted in the shorter experimental cell, and had a flow rate of 0.26 $mm^3\,s^{-1}$. The absence of fine salt powder behind the reaction front leads to very clear change in light intensity at the reaction front, as shown by the arrows. The injected water is initially dyed blue, but this is changed to red later in the experiment. The dye suggests that the most recently injected fluid spreads rapidly through the reacted zone, and then gradually advances across the reaction front, which thereby migrates forwards.

fluid spreads rapidly through the reacted zone of higher permeability, and then gradually advances across the reaction front, which thereby deepens and migrates forwards. In each experiment, as the flow continued, the reaction zone spread along the upper side of the cell, dissolving away a channel of high permeability.

In order to compare the model with the experimental results, we have generated a series of profiles of the reaction front depth as a function of time. One typical set of results for the long experimental cell, shown as the symbols in figure 4, correspond to an experiment in which the volume flux of fresh water supplied to the tank was 0.15 $m^3\,s^{-1}$, and in which the volume fraction of salt in the porous layer was initially 5 %. The reaction front profiles are shown at dimensionless times 6.7, 10.1, 13.5 and 16.9 (see below) corresponding to the actual times 1200, 1800, 2400 and 3000 s after the start of the experiment. The reaction front extends over 160 cm along the tank by the time of the fourth profile. In order to compare these experimental observations with the predictions of the model (7), we require estimates for the values of the parameters β, B and λ for this experiment. First, based on the calibration experiments, the ratio

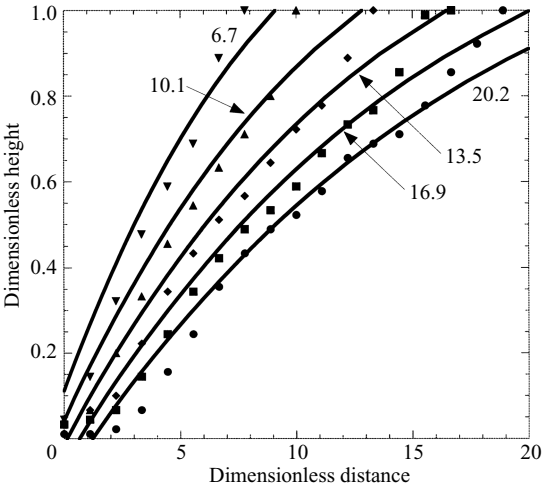

FIGURE 4. Comparison of the predictions of the theoretical model (solid lines) with laboratory measurements (symbols) of the dimensionless location of the reaction front, at the dimensionless times 6.7, 10.1 13.5 and 16.9 during an experiment. These data were collected from the long experimental cell with an injection rate of $0.15\,\mathrm{mm^3\,s^{-1}}$. In comparing the model with the experimental data, we use the values $\lambda = 1.54$, $B = 2.1$, and $\beta \sim 2.0$, estimated from the input conditions or calibration experiments conducted prior to the main experiment, as described in the text.

of the fluid mobility in the unreacted and reacted zones was taken to be $\beta = 2.0$. Secondly, we estimated that the porosity of the cell was $\phi \sim 0.4$ and the unreacted matrix had permeability $1.85 \times 10^{-10}\,\mathrm{m^2}$. Since the saturated aqueous solution in equilibrium with the reactive porous layer contained about 25 wt % salt, then we estimate that $B = 2.1$. Thirdly, comparison of the area of reacted matrix behind the reaction front with the volume of injected fluid, as estimated from the experimental reaction front profiles at the four times (figure 4), suggests that the reaction parameter λ (equation (3)) has value 1.55 ± 0.05. This is consistent with the model prediction $\lambda \sim 1.54$ based on equation (3). Using the values for the parameters β, B and λ, as estimated above, we then solved numerically the model equation (7) to calculate the dimensionless shape of the interface at the dimensionless times 6.75, 10.1, 13.5 and 16.9. The numerical predictions (solid lines) are compared with the observed shape of the reaction fronts (symbols) at the four times shown in figure 4. It is seen that, as a leading-order description of the process, the model predictions are in reasonable agreement with the experimental observations. There are some differences however, especially at the lower boundary of the cell. These may in part be the result of the rather simplified model of a localized, stable and well-defined reaction front.

4. Axisymmetric geometry

The modelling and experiments in §§2 and 3 focused on planar flows, as would correspond to injection of water into a horizontal well, or the leakage of water from a fracture cutting through an aquifer. As described in §2, for constant injection, the full governing equation requires numerical solution. However, assuming the reaction front remains stable and spreads axisymmetrically under the upper boundary of the aquifer, as in the two-dimensional experiments, then there are asymptotic solutions

in the limit of small B, and these solutions identify the important role of the change in fluid mobility, β, in the evolution of the reaction front.

In contrast to the horizontal well, if liquid is injected from a vertical well and spreads axisymmetrically then, for a fixed injection rate, the flow speed decreases with distance. Now the motion becomes self-similar, as in the somewhat analogous flow of a confined gravity current (Mitchell & Woods 2006; Nordbotten & Celia 2006). Such similarity solutions can provide a valuable complement to the one-dimensional analysis, and we therefore now explore the behaviour of such a gravity-driven, axisymmetric reaction front.

From a similar derivation to that given in § 2, it follows that for steady injection through a central vertical well, at flow rate Q, into a confined reacting layer of rock, the height of the reaction zone above the base of the layer h takes the form (cf. equation (7))

$$r\frac{\partial(H-h)}{\partial t}+\frac{\beta\lambda Q}{2\pi H}\frac{\partial}{\partial r}\left[\frac{H-h}{h+(H-h)\beta}\right]=-\frac{\lambda k_u\Delta\rho g}{\mu_u}\frac{\partial}{\partial r}\left[\frac{h(H-h)r}{h+(H-h)\beta}\frac{\partial h}{\partial r}\right]. \quad (11)$$

This equation admits solutions of the form $h=H(1-\mathscr{F}(\eta))$ where

$$\eta=r\left(\frac{2\pi H}{\lambda\beta Qt}\right)^{1/2} \quad (12)$$

and $\mathscr{F}$, the dimensionless depth of the reacted zone, satisifies the ordinary differential equation

$$\left[\left(\frac{1}{1+(\beta-1)\mathscr{F}}\right)^2-\frac{\eta^2}{2}\right]\frac{\mathrm{d}\mathscr{F}}{\mathrm{d}\eta}=B_r\frac{\mathrm{d}}{\mathrm{d}\eta}\left[\frac{\eta\mathscr{F}(1-\mathscr{F})}{1+(\beta-1)\mathscr{F}}\frac{\mathrm{d}\mathscr{F}}{\mathrm{d}\eta}\right] \quad (13)$$

where

$$B_r=\frac{2\pi k_l\Delta\rho g H^2}{\mu_l Q}.$$

Also, $\mathscr{F}$ satisfies the boundary conditions that at the outer edge of the reaction front, where $\eta=\lambda_2$, then $\mathscr{F}(\lambda_2)=0$ and

$$\frac{\mathrm{d}\mathscr{F}}{\mathrm{d}\eta}=\frac{2-\lambda_2^2}{2B_r\lambda_2}. \quad (14)$$

At the inner edge of the reaction front, where $\eta=\lambda_1$, then $\mathscr{F}(\lambda_1)=1$ and

$$\frac{\mathrm{d}\mathscr{F}}{\mathrm{d}\eta}=\frac{\beta^2\lambda_1^2-2}{2B_r\lambda_1\beta}. \quad (15)$$

This latter condition requires that $\lambda_1<2^{1/2}/\beta$. Again, there are two control parameters for the flow, B_r and β. In figure 5, we present a range of solutions for the shape of the reaction front as a function of B_r (figure 5*a*), and the mobility ratio β (figure 5*b*). It may be seen that as B_r increases, so that the buoyancy contrast across the reaction front dominates the radial pressure gradient associated with the flow, then the flow tends to spread out more rapidly along the upper surface of the layer. Similarly, as β increases, corresponding to a larger permeability contrast across the reaction front, the reaction front tends to form a much more focused channel along the top of the layer.

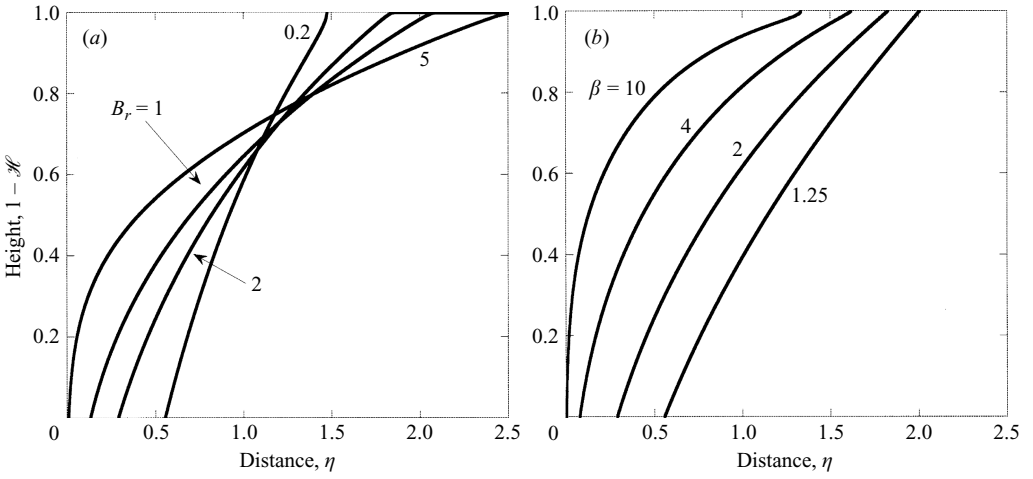

FIGURE 5. Variation of the shape of the self-similar axisymmetric reaction front as a function of distance from the source for a range of values of (*a*) B_r, the buoyancy parameter, and (*b*) β, the mobility ratio across the reaction front.

By analogy with equations (7) and (10), in the limit of relatively weak buoyancy force, $B_r \to 0$, equation (13) has the limiting analytic solution

$$\mathscr{F} = \frac{1}{\beta - 1}\left(\frac{2^{1/2}}{\eta} - 1\right) \quad \text{for} \quad \left(2^{1/2}/\beta\right) < \eta < 2^{1/2}. \tag{16}$$

This theoretical solution, which is based on the assumption that the reaction front remains as a stable intrusion, spreading along the upper boundary of the layer (see discussion in § 2), illustrates that the leading edge of the reaction front has position $\eta = 2^{1/2}$ which has dimensional value $r = (\lambda\beta Qt/(\pi H))^{1/2}$. This is a factor $\beta^{1/2}$ further than a purely vertical axisymmetric reaction front would propagate, indicating the importance of the mobility ratio in dispersing the reaction front. Figure 5(*a*) illustrates that with $B_r > 0$ so that the current also spreads under gravity, then the leading edge of the reaction front advances even more rapidly from the source. It is interesting to compare this result with the two-dimensional case (§ 2), in which the theoretical solution (10) suggests that the current would advance a factor β further than the purely vertical front (in the limit $B \to 0$).

5. Discussion

We have investigated both experimentally and theoretically the effect of a dissolution reaction on the propagation of a buoyant reactive fluid through a confined porous rock. Our simplified analytical model provides new insight into the controls on the rate of propagation of gravity-controlled reaction fronts, and is in reasonable accord with our experimental results. The model identifies how the increase of the permeability of the matrix as a result of the reaction can increase the mobility and hence the spreading rate of the buoyant reactive fluid and the reaction front. It also illustrates how the buoyancy force arising from a change in fluid density across the reaction front acts to disperse the reactive fluid and hence the leading edge of the reaction front even further. The reaction may therefore substantially enhance the lateral spreading of the injected liquid, and can lead to dissolution of a relatively fine and laterally extensive channel through the rock.

Given the uncertainties in highly complex geological systems, simplified quantitative models such as that proposed herein provide valuable constraints for interpreting the processes leading to the formation of very extensive mineral reaction zones associated with fluid flow. Examples of such reaction zones include those observed in carbonates and other reactive geological deposits (Liu *et al.* 1997; Phillips 1991). Data from laboratory experiments on reactions in rock suggest that the mobility ratio across a reaction front may have a value as large as 10–100 (Grigg *et al.* 2003). Even with axisymmetric flow, this may then lead to the reaction front and the fluid being dispersed a factor 3–10 times further than if we assume the reaction front is vertical, and perhaps as much as 100 times further in an axisymmetric flow. Such dynamic dispersion can help to rationalize the very significant lateral extent of some reaction zones in some carbonate rocks (Phillips 1991), which would not be possible through purely diffusive transport of reactants.

However, several caveats should be noted concerning the present modelling. First, it should be noted that the heterogeneity of real rock formations may be responsible for some of the dispersion of a reaction front in real rocks, and this can affect the spreading rate of the front. Also, in the present modelling, we have assumed that the reaction front remains stable and well-defined, as observed in our analogue experiments. However, pressure-driven dissolution fronts in reactive porous media can become unstable (Ortoleva *et al.* 1987), leading to intricate fingering and wormhole formation (e.g. Golfier *et al.* 2002); such phenomena are beyond the scope of the present work, in which the buoyancy of the reactive fluid leads to a stable advancing reaction front (figures 1, 3*b*), but such effects are likely to arise when the buoyancy parameter B is small, as occurs if either (i) the flow rate increases or (ii) the buoyancy of the reactive fluid decreases (equation (8)). We plan to explore this different reaction regime, and its dependence on B and β in more detail, both experimentally and theoretically. In particular, it will be interesting to explore whether the much smaller cross-front length scales associated with a fingering interface leads to diffusive mixing and a reduction in the rate of propagation of the reaction zone, as implied by the recent analysis of Yortsos & Salin (2006).

This work has been supported by the BP Institute in University of Cambridge. The paper was greatly improved by a series of very helpful referees reports.

REFERENCES

Ames, W. F. 1977 *Numerical Methods for Partial Differential Equations.* Academic.

Barenblatt, G. 1996 *Dimensional Analysis, Self-Similarity and Intermediate Asymptotics.* Cambridge University Press.

Bear, J. 1972 *Dynamics of Flow in Porous Media.* Elsevier.

Chen, Y., Fambrough, J., Bartko, K., Li Y., Montgomery, C. & Ortoleva, P. 1997 Reaction-transport simulation of matrix acidizing and optimal acidizing strategies. SPE 37282, *SPE Intl Symp. on Oilfield Chem., Houston.*

Daccord, G., Lenormand, R. & Lietard, O. 1993*a* Chemical dissolution of a porous medium by a reactive fluid – I Model for the wormholing phenomenon. *Chem Engng Sci.* **48**, 169–178.

Daccord, G., Lenormand, R. & Lietard, O. 1993*b* Chemical dissolution of a porous medium by a reactive fluid – II convection vs. reaction behaviour diagram. *Chem Engng Sci.* **48**, 179–186.

Fredd, C. N. & Fogler, H. S. 1999 Optimum conditions for wormhole formation in carbonate porous media: Influence of transport and reaction. *SPE J.* 4(3).

Golfier, F., Zarcone, C., Bazin, B., Lenormand, R., Lasseux, D. & Quitard, M. 2002 On the ability of a Darcy scale model to capture wormhole formation during the dissolution of a porous medium. *J. Fluid Mech.* **457**, 213–254.

Grigg, R., McPherson, B. & Svec, R. 2003 Laboratory and model tests at reservoir conditions for CO_2-brine-carbonate rock systems interactions. *The Second Annual DOE Carbon Sequestration Conference, May 5–8, 2003, Washington, D.C.*

Jupp, T. & Woods, A. W. 2003 Thermally driven reaction fronts in porous media. *J. Fluid Mech.* **484**, 329–346.

Jupp, T. & Woods, A. W. 2004 Reaction fronts in a porous medium following injection along a temperature gradient. *J. Fluid Mech.* **513**, 343–361.

Lagneau, V., Pipart, A. & Catalette, H. 2005 Reactive transport modelling and long term behaviour of CO_2 sequestration in saline aquifers, oil and gas science and technology. *Rev. Inst. Petrol. Fr.* (IFP) **60**(2), 231–247.

Liu, X., Ormond, A., Bartko, K., Li, Y. & Ortoleva, P. 1997 A geochemical reaction-transport simulator for matrix acidizing analysis and design. *J. Petrol. Sci. Engng* **17**, 181–196.

Menand, T., Raw, A. & Woods, A. W. 2003 Thermal inertia and reversing buoyancy in flow in porous media. *Geophys. Res. Lett.* **30**, 1291–1293.

Mitchell, V. & Woods, A. W. 2006 Self-similar dynamics of liquid injected into partially saturated aquifers. *J. Fluid Mech.* **566**, 345–355.

Nigam, M. S. & Woods, A. W. 2006 The influence of buoyancy contrasts on source-sink flows in a porous media with thermal inertia. *J. Fluid Mech.* **549**, 253–271.

Nordbotten, J. M. & Celia, M. A. 2006 Similarity solutions for fluid injection in confined aquifers. *J. Fluid Mech.* **561**, 307–327.

Ortoleva, P., Merino, E., Moore, C. & Chadam, J. 1987 Geochemical self-organization. Part II. The reactive-infiltration instability. *Am. J. Sci.* **287**, 1008–1040.

Phillips, O. M. 1991 *Flow and Reactions in Permeable Rocks.* Cambridge University Press.

Raw, A. & Woods, A. W. 2003 On gravity driven flow through a reacting porous rock. *J. Fluid Mech.* **474**, 227–243.

Woods, A. W. 1999 Liquid and vapour flows in porous rocks. *Annu. Rev. Fluid Mech.* **31**, 171–199.

Yortsos, Y. C. & Salin, D. 2006 On the selection principle for viscous fingering in porous media. *J. Fluid Mech.* **557**, 225–236.